Computer Physics Communications 181 (2010) 837–841

Contents lists available at ScienceDirect

Computer Physics Communications

www.elsevier.com/locate/cpc

Spectral element spatial discretization error in solving highly anisotropic heat conduction equation

E.T. Meier [a,*], V.S. Lukin [b], U. Shumlak [a]

[a] Plasma Science and Innovation Center, University of Washington, Seattle, WA 98195-2250, USA
[b] Space Sciences Division, Naval Research Laboratory, Washington, DC 20375, USA

ARTICLE INFO

Article history:
Received 2 May 2009
Received in revised form 18 November 2009
Accepted 24 December 2009
Available online 4 January 2010

Keywords:
Anisotropy
High order
Spectral element
Finite element
Numerical error
Perpendicular diffusion

ABSTRACT

This paper describes a study of the effects of the overall spatial resolution, polynomial degree and computational grid directionality on the accuracy of numerical solutions of a highly anisotropic thermal diffusion equation using the spectral element spatial discretization method. The high-order spectral element macroscopic modeling code SEL/HiFi has been used to explore the parameter space. It is shown that for a given number of spatial degrees of freedom, increasing polynomial degree while reducing the number of elements results in exponential reduction of the numerical error. The alignment of the grid with the direction of anisotropy is shown to further improve the accuracy of the solution. These effects are qualitatively explained and numerically quantified in 2- and 3-dimensional calculations with straight and curved anisotropy.

1. Introduction

Modeling in the presence of significant anisotropy is required in a variety of fields including image processing [1], electromagnetics [2], medical imaging [3], geological science [4], and plasma science [5].

When modeling anisotropic behavior with low-order spatial discretization schemes, prohibitively high spatial resolution is often required to achieve the desired degree of accuracy. As demonstrated below, local grid alignment with the direction of anisotropy reduces resolution requirements. However, in systems where the field representing the anisotropy is topologically complex, only approximate grid alignment is possible and solution representations with exponential spatial convergence rates may be necessary. High-order spectral element representations [6] meet this need. Increasing element order allows a reduction of total degrees of freedom to reach a given accuracy, and can often lead to an improvement of overall computational efficiency [7]. The work presented here, focusing on anisotropic thermal diffusion and conducted with the SEL/HiFi high-order spectral element macroscopic modeling code [8–10], clearly demonstrates the expected reduction in total degrees of freedom and exponential convergence. Also, the effect of grid alignment on accuracy is quantified.

In magnetic confinement fusion device simulations, it is particularly important to properly capture thermal diffusion anisotropy. In these systems, characteristic rates of heat conduction parallel and perpendicular to the local direction of magnetic field can differ by as many as nine orders of magnitude and any spurious leakage of parallel heat flow into the perpendicular direction would destroy the simulations' predictive capabilities [5]. Complex magnetic topologies which preclude grid alignment occur in tokamak edge plasmas and in other devices when islands or regions of ergodic field are present. For an example of a successful high-order finite element computation involving complex magnetic topology and strong anisotropy, see the non-linear tearing mode evolution study in [5].

It should be noted that special methods have been proposed to allow low-order elements to accurately capture anisotropic behavior — see [11], for example. However, the present research concentrates on developing a computational framework that is broadly applicable.

Three anisotropic thermal diffusion test problems are described in Section 2. These problems are designed to explore straight anisotropy in two and three dimensions and curved anisotropy in two dimensions. In Section 3, error in modeling anisotropic diffusion is briefly discussed from an analytical standpoint to provide an intuitive picture of the source of inaccuracy in the results. Results are presented and discussed in Section 4, and, finally, the main points are summarized in Section 5.

* Corresponding author.
E-mail address: etmeier@u.washington.edu (E.T. Meier).

0010-4655/$ – see front matter
doi:10.1016/j.cpc.2009.12.018

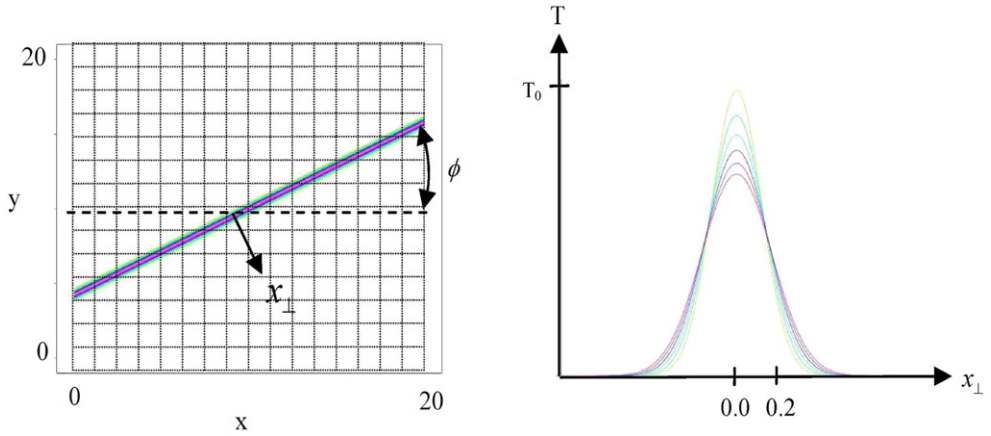

Fig. 1. Setup for test problem one (TP1). On the left is the domain and initial condition with temperature contours shown. Plotted on the right are slices of temperature perpendicular to the anisotropy as time progresses. (The decrease in peak temperature is exaggerated for illustration.) Initial peak temperature is $T_0 = 1$. The Gaussian profile is always centered at $x = 10$, $y = 10$.

2. Test problem descriptions

2.1. Thermal diffusion model

The equation studied is the thermal diffusion equation,

$$\frac{\partial T}{\partial t} + \nabla \cdot (-\overleftrightarrow{\mathbf{D}} \cdot \nabla T) = 0. \tag{1}$$

Here, T is temperature, and $\overleftrightarrow{\mathbf{D}}$ is the anisotropic thermal conductivity tensor. In 3D,

$$\overleftrightarrow{\mathbf{D}} = \begin{pmatrix} D_\parallel \cos^2(\phi) + D_\perp \sin^2(\phi) & (D_\parallel - D_\perp)\sin(\phi)\cos(\phi) & 0 \\ (D_\parallel - D_\perp)\sin(\phi)\cos(\phi) & D_\parallel \sin^2(\phi) + D_\perp \cos^2(\phi) & 0 \\ 0 & 0 & D_\perp \end{pmatrix},$$

where $D_\parallel$ and $D_\perp$ are parallel and perpendicular heat conduction coefficients, and ϕ is the angle in the x–y plane from the positive x-direction to the direction of high parallel conductivity. $\phi = 0°$ indicates perfect alignment of the grid with the anisotropy. In 2D, $\overleftrightarrow{\mathbf{D}}$ reduces to the 2-by-2 tensor in the upper left of the 3-by-3 3D tensor.

2.2. Domain and initial condition

The domain and initial condition for test problem one (TP1) are shown in Fig. 1. Perpendicular to the direction of anisotropy, the temperature profile is a Gaussian: $T = \exp(-x_\perp^2/\lambda^2)$ where $x_\perp$ is the distance from the Gaussian peak, and λ is the characteristic width of the Gaussian. Note that the peak temperature is one. The initial analytical temperature profile is uniform in the direction of anisotropy. The domain is square with 20 length units per side, and the characteristic width of the Gaussian temperature profile is 0.2. The relatively large domain size makes boundary effects negligible. Grid alignment is varied from 0 to 60 degrees. (As expected, results for $\phi = 60°$ are identical to results when $\phi = 30°$.)

Test problem two (TP2) is similar to TP1 except that the domain is 3D such that isosurfaces of the Gaussian temperature profile are cylindrical. Fig. 2 shows the problem setup. The direction of high parallel thermal conductivity is rotated 30 degrees from the x-direction in the x–y plane ($\phi = 30°$). The grid alignment is not varied. This problem demonstrates the spectral element performance in 3D. As in TP1, the characteristic width of the Gaussian temperature profile is 0.2. The x–y domain is a 10-by-10 square. (In TP1, a 20-by-20 square is used; TP2 is more computationally demanding, and a 10-by-10 domain is found to sufficiently remove boundary effects.) Rotation of the Gaussian occurs only in the x–y plane and the chosen z-direction domain extent of 2 units is large enough to prevent boundary effects.

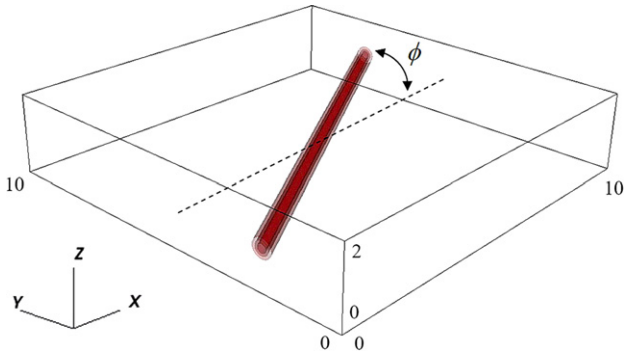

Fig. 2. Setup for test problem two (TP2). Temperature is shown in nested semi-transparent red isosurfaces. The Gaussian temperature profile is cylindrical instead of linear as on TP1. Initial peak temperature is $T_0 = 1$. The mesh is composed of cubic grid cells. The angle of the Gaussian to the anisotropy is fixed at $\phi = 60°$. (For interpretation of color in this figure, the reader is referred to the web version of this article.)

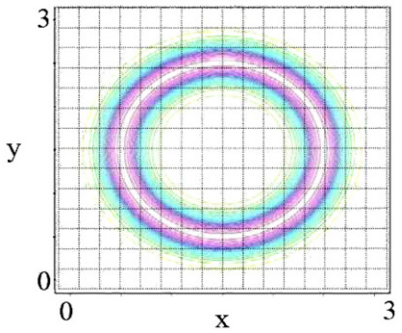

Fig. 3. Setup for test problem three (TP3). Temperature contours are shown. Initial peak temperature is $T_0 = 1$. The peak of the Gaussian profile is 1 unit from the center of the domain.

The test problem three (TP3) initial condition is shown in Fig. 3. In this 2D problem, the Gaussian peak is a function of radius from the center of the domain. The Gaussian peak is at 1 unit from the center and the characteristic width is 0.2 as in TP1 and TP2. As shown in Fig. 3, this forms a circular "ridge" of high temperature. The anisotropy is aligned in the polar direction, that is, aligned with the circular temperature contours. The x–y domain is a 3-by-3 square — large enough to prevent boundary effects.

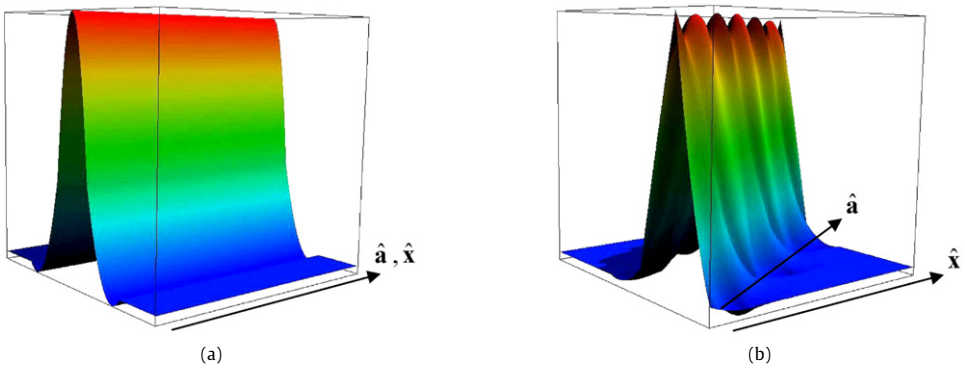

(a) (b)

Fig. 4. In (a) and (b), the Gaussian temperature profile is poorly resolved with $h = 0.4$, and $np = 2$. $\hat{\mathbf{x}}$ indicates the Cartesian direction of grid orientation and $\hat{\mathbf{a}}$ is the direction of anisotropy. When the grid is aligned as in (a), the profile does not vary in the parallel direction. In (b), the grid is misaligned by $\phi = 30°$, and the temperature profile varies in the parallel direction and numerical perpendicular diffusion occurs.

2.3. Boundary conditions

A zero flux boundary condition,

$$\hat{\mathbf{n}} \cdot (\overleftrightarrow{\mathbf{D}} \cdot \nabla T) = 0, \tag{2}$$

is applied to all boundaries (edges in the 2D problems and surfaces in the 3D problem), implying that the domain is perfectly insulating.

2.4. Resolution

Resolution in the x-, y- and z-directions is identical in these simulations. The range of polynomial degree (np) studied is $np = 2$ to 6. Element size (h) ranges from approximately 0.07 to 0.33. The number of degrees of freedom per unit length (dof) is useful in comparisons, and is defined to be $dof = nx * np$, where nx is the number of elements per unit length (and $nx = ny$). $dof = 18$, 24, and 30 are studied.

2.5. Time evolution

Data is collected with uniform, constant parallel thermal conductivity ($D_{\parallel} = 1$) and zero perpendicular thermal conductivity ($D_{\perp} = 0$). When numerical error allows leakage in the transverse direction, the Gaussian profile diffuses. The total simulation duration for all runs is 10 time units.

3. Analytical considerations

Though not mathematically rigorous, the following analysis provides an intuitive feel for the source of numerical perpendicular thermal diffusion.

For finite elements representations of order np, error is of order $O(h^{np+1})$, provided the following conditions are met [12]: the converging quantity is well behaved, i.e. has finite strain energy; the basis functions are sufficiently uniform; the solution is sufficiently smooth. Because SEL/HiFi, a C^0-continuous spectral element code, solves PDEs in weak form such that only first derivatives of dependent variables are needed, the strain energy constraint is satisfied globally. The requirements on basis function uniformity and solution smoothness are easily met in the simulations for this work which involve rectangular (and hexahedral) cells with fixed aspect ratio and infinitely differentiable Gaussian profiles. In realistic applications, the challenges of maintaining solution smoothness and basis function uniformity require attention to mesh generation and provision of sufficient spatial resolution (perhaps via mesh adaptation).

The source of perpendicular numerical diffusion error due to anisotropy is best understood by rewriting Eq. (1) in terms of a numerical solution, $\tilde{T} = T - \delta T$, where T is a solution that exactly satisfies $\nabla \cdot (-\overleftrightarrow{\mathbf{D}}_{\parallel} \cdot \nabla T) = 0$, where $\overleftrightarrow{\mathbf{D}}_{\parallel}$ is just $\overleftrightarrow{\mathbf{D}}$ with $D_{\perp} = 0$, and δT is the numerical error of order $O(h^{np+1})$. Setting $D_{\perp} = 0$, the evolution equation for $\tilde{T}$ is

$$\frac{\partial \tilde{T}}{\partial t} + \nabla \cdot (-\overleftrightarrow{\mathbf{D}}_{\parallel} \cdot \nabla \tilde{T}) = 0,$$

or equivalently,

$$\frac{\partial \tilde{T}}{\partial t} + \nabla \cdot \left(-\overleftrightarrow{\mathbf{D}}_{\parallel} \cdot \nabla(-\delta T)\right) = 0.$$

The finite element gradient operators are analytically exact, and the tensor $\overleftrightarrow{\mathbf{D}}_{\parallel}$ is also analytically specified. Therefore, diffusion can arise only due to the numerical error, δT, in representing the temperature itself.

As illustrated in Fig. 4, for a uniform anisotropy as in the first test problem, numerical error only arises when the computational mesh is misaligned with the anisotropy. The same relatively low-resolution mesh is used in Fig. 4(a) and (b). When the computational mesh is aligned with the anisotropy, as in Fig. 4(a), the same (flawed) perpendicular temperature profile is perfectly replicated at all parallel locations, and $\nabla_{\parallel} \delta T = 0$ everywhere. However, if the computational mesh is not aligned, as in Fig. 4(b), the perpendicular profile is different at various parallel locations and $\nabla_{\parallel} \delta T \neq 0$.

4. Results and discussion

Numerical error is evaluated by evolving the solution for a fixed total time, and then comparing the final maximum temperature in the domain (T_{final}) to the initial maximum temperature (T_0). All simulations are fully resolved in time. Parallel conductivity is unity for all results. To relate $\Delta T_{num.} \equiv T_0 - T_{final}$ to actual perpendicular diffusion, ΔT_{real} is computed for a range of non-zero $D_{\perp}$ values. These calculations are fully spatially resolved. Fig. 5 shows ΔT_{real} vs. $D_{\perp}$ for TP1. In simulations with $D_{\perp} = 0$, numerical perpendicular diffusion error can cause a non-zero $\Delta T_{num.}$. A power fit equation relating $D_{\perp}$ to ΔT_{real} is found and used to convert $\Delta T_{num.}$ to an effective numerical diffusion, $D_{\perp,num.}$. Note that parallel conductivity is unity for all results. This approach is used to determine effective numerical diffusion, $D_{\perp,num.}$, as a function of $\Delta T_{num.}$ for all three test problems.

Fig. 6 shows results from TP1. $D_{\perp,num.}$ is plotted for $\phi = 5°$ to 60° for $dof = 24$. Equivalent plots for $dof = 18$ and 30 are omitted, but show similar trends. As shown, $D_{\perp,num.} \to 0$ as $\phi \to 0°$.

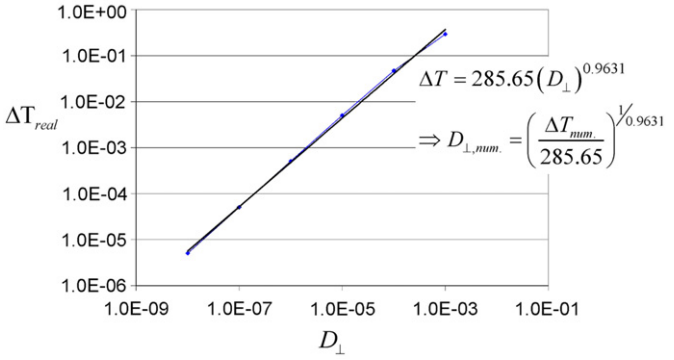

Fig. 5. ΔT_{real}, the final maximum temperature minus initial maximum temperature due to non-zero simulated transverse conductivity, is plotted vs. $D_\perp$. Results are from fully resolved simulations (in space and time). This data is used to define numerical perpendicular diffusion, $D_{\perp,num.}$, given a $\Delta T_{num.}$ found in simulations with $D_\perp = 0$. The data shown is for TP1. A similar approach is used to define $D_{\perp,num.}$ for all three test problems.

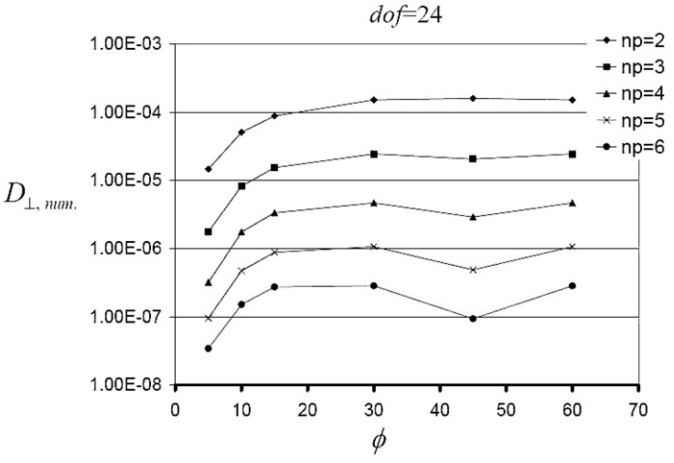

Fig. 6. Numerical perpendicular diffusion versus ϕ for $np = 2$ to 6 with $dof = 24$. (At $\phi = 0°$, $D_{\perp,num.}$ is exactly zero and cannot be plotted on the log scale.) Increasing np at a given dof provides the expected exponential reduction of error.

The dip in $D_{\perp,num.}$ near $\phi = 45°$ indicates an enhanced accuracy when the anisotropy approaches alignment with one of the two diagonals of each cell. This enhancement could be related to the symmetry across the diagonals.

Grid alignment is fixed to $\phi = 30°$ in Fig. 7 and the effect of element size on $D_{\perp,num.}$ is presented for $np = 2$ to 6. Results for other grid alignment angles show similar trends. Refining polynomial degree at fixed element size results in an exponential reduction in $D_{\perp,num.}$. Theoretical predictions outlined in Section 3, also shown in Fig. 7, predict slightly slower convergence rates than seen in the simulation results, especially for high np. In Figs. 8 and 9, similar results are shown for TP2 and TP3, respectively. Grid alignment is $\phi = 30°$ for the TP2 results and there is, of course, no alignment in the TP3 results which involve curved anisotropy.

As illustrated by the data, high np allows a given accuracy with significantly fewer total degrees of freedom. This result is valid not only for 2D problems with straight anisotropy as shown in Fig. 7, but also for 3D problems and for curved anisotropy, as shown in Figs. 8 and 9. For example, in Fig. 7, with $np = 5$ and $dof = 18$, $D_{\perp,num.} = 10^{-5}$ while with $np = 3$, $dof = 30$ is required to reach the same accuracy. By reducing the total number of degrees of freedom, high-order accuracy methods offer reduced memory requirements. Overall computational efficiency is also improved in many applications — for example, in [7] it is shown that computational efficiency is improved for long-time simulations of unsteady flows.

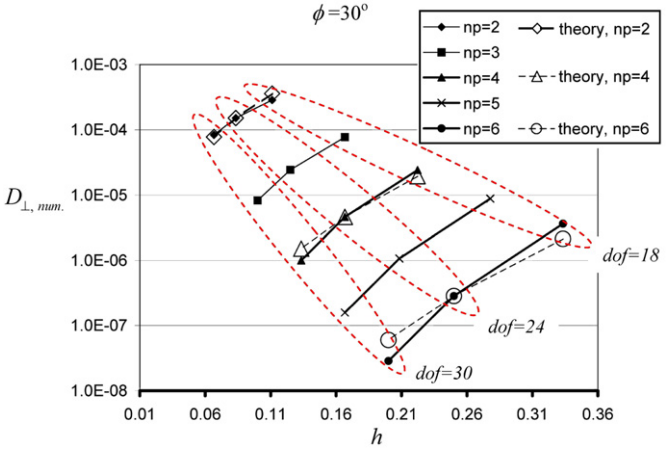

Fig. 7. TP1 (2D straight anisotropy): Numerical perpendicular diffusion vs. h for various np at $\phi = 30°$. Data points corresponding to $dof = 18$, 24, and 30 are indicated by the dashed ellipses. The effect of np can be seen for constant h: at h 0.17, increasing np from 3 to 5 reduces $D_{\perp,num.}$ by two orders of magnitude. Theoretical predictions based on $O(h^{np+1})$ scaling are provided for $np = 2$, 4, and 6. The theoretical predictions are scaled to match the simulation data for $dof = 24$.

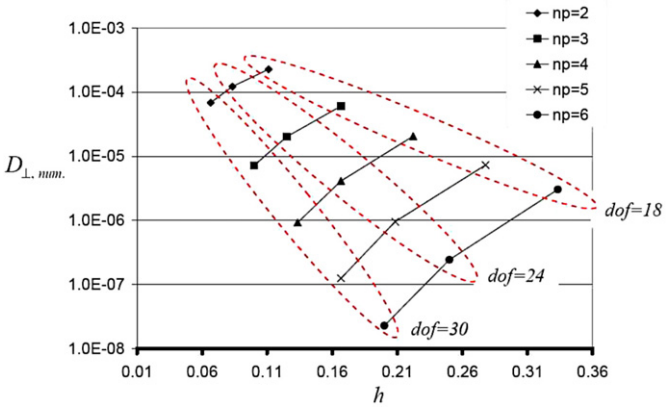

Fig. 8. TP2 (3D straight anisotropy): Numerical perpendicular diffusion vs. h for various np. Data points corresponding to $dof = 18$, 24, and 30 are indicated by the dashed ellipses. Convergence trends are very similar to trends for TP1.

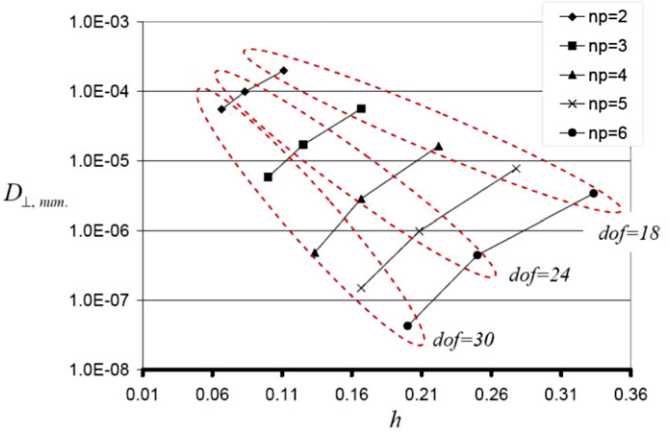

Fig. 9. TP3 (2D curved anisotropy): Numerical perpendicular diffusion vs. h for various np. Data points corresponding to $dof = 18$, 24, and 30 are indicated by the dashed ellipses. Convergence trends are very similar to trends for TP1.

5. Conclusions

By modeling anisotropic heat conduction with a spectral element technique, it has been shown that high-order elements yield a given accuracy with less total degrees of freedom than lower-order elements. Similar results are found for problems in 2D and 3D and for straight and curved anisotropy. Convergence with grid alignment has been explored, and results show that even small grid misalignment cause significant numerical error. This error can be efficiently controlled by using high-order spectral spatial representation.

In the study of grid alignment error, a subtlety has been found in which accuracy improves near a 45° alignment angle. Some grid adaptation schemes (like the one implemented for SEL/HiFi) use grid refinement algorithms based on error minimization, and the fact that there is a local minimum in numerical error due to grid misalignment should be noted.

Theoretical predictions of numerical diffusion error are presented and, for a given grid alignment, these predictions are in good agreement with computed results. Error estimates that take grid alignment into account have not been made.

Employing spectral element representations may be beneficial in fields as diverse as fusion science, image processing, and medical imaging. For example, high-order finite element techniques are gaining favor in electromagnetic wave modeling where direction-dependent numerical dispersion error must be controlled [2,13]. The present research provides a basis for quantifying the benefits of the spectral element approach when modeling anisotropic behavior.

Acknowledgements

This research is supported by DOE grant number DE-FC02-05ER54811. Computational resources for the research include the Bassi IBM p575 POWER 5 system at NERSC, the PSI-Center SGI Altix 350 cluster, and the PSI-Center SGI ICE Altix 8200 cluster.

References

[1] P. Perona, J. Malik, Scale-space and edge detection using anisotropic diffusion, IEEE Trans. Pattern Anal. Machine Intell. 12 (1990) 629.
[2] G. Sun, C.W. Trueman, Suppression of numerical anisotropy and dispersion with optimized finite-difference time-domain methods, IEEE Trans. Antennas and Propagation 53 (2005) 4121.
[3] P.J. Basser, D.K. Jones, Diffusion-tensor MRI: Theory, experimental design, and data analysis – a technical review, NMR Biomed. 15 (2002) 456.
[4] M. Saadatfar, M. Sahimi, Diffusion in disordered media with long-range correlations: anomalous, Fickian, and superdiffusive transport and log-periodic oscillations, Phys. Rev. B 65 (2002) 036116.
[5] C.R. Sovinec, et al., Nonlinear magnetohydrodynamics simulation using high-order finite elements, J. Comput. Phys. 195 (2004) 355.
[6] R.D. Henderson, Adaptive spectral element methods for turbulence and transition, in: T.J. Barth, H. Deconinck (Eds.), High-Order Methods for Computational Physics, Springer-Verlag, New York, 1999.
[7] H.O. Kreiss, Numerical Methods for Solving Time-Dependent Problems for Partial Differential Equations, Presses de l'Université de Montréal, Montreal, QC, 1978.
[8] A.H. Glasser, X.Z. Tang, The SEL macroscopic modeling code, Comput. Phys. Comm. 164 (2004) 237.
[9] V.S. Lukin, Computational study of the internal kink mode evolution and associated magnetic reconnection phenomena, PhD thesis, Princeton University, 2007.
[10] V.S. Lukin, A.H. Glasser, W. Lowrie, E.T. Meier, Overview of HiFi – implicit spectral element code framework for general multi-fluid applications, J. Comput. Phys. (2009), submitted for publication.
[11] S. Günter, et al., Finite element and higher order difference formulations for modelling heat transport in magnetised plasmas, J. Comput. Phys. 226 (2007) 2306.
[12] G. Strang, G.J. Fix, An Analysis of the Finite Element Method, Prentice–Hall, Englewood Cliffs, NJ, 1973.
[13] J. Jin, The Finite Element Method in Electromagnetics, Wiley, New York, 2002.